# Facile Synthesis of Gold Nanoparticles with Alginate and Its Catalytic Activity for Reduction of 4-Nitrophenol and H$_2$O$_2$ Detection

**Xihui Zhao [1,2,\*], Zichao Li [3], Yujia Deng [1], Zhihui Zhao [1,2], Xiaowen Li [1] and Yanzhi Xia [2,3,\*]**

[1]   School of Chemistry and Chemical Engineering, Qingdao University, Qingdao 266071, China; dengyujia@qdu.edu.cn (Y.D.); zzh@qdu.edu.cn (Z.Z.); xiaowenli@qdu.edu.cn (X.L.)

[2]   Collaborative Innovation Center for Marine Biomass Fibers, Materials and Textiles of Shandong Province, Institute of Marine Bionbased Materials, Qingdao University, Qingdao 266071, China

[3]   State Key Laboratory Breeding Base of New Fiber Materials and Modern Textile, School of Materials Science and Engineering, Qingdao University, Qingdao 266071, China; zichaoli@qdu.edu.cn

\*   Correspondence: zhaoxihui@qdu.edu.cn (X.Z.); xiayzh@qdu.edu.cn (Y.X.); Tel.: +86-532-8595-0705 (X.Z.)

**Abstract:** Gold nanoparticles (AuNPs) were synthesized using a facile solvothermal method with alginate sodium as both reductant and stabilizer. Formation of AuNPs was confirmed by UV-vis spectroscopic analysis. The synthesized AuNPs showed a localized surface plasmon resonance at approximately 520–560 nm. The AuNPs were characterized using transmission electron microscopy, X-ray diffraction and dynamic light scattering. Transmission electron microscopy revealed that the AuNPs were mostly nanometer-sized spherical particles. Powder X-ray diffraction analysis proved the formation of face-centered cubic structure of Au. Catalytic reduction of 4-nitrophenol was monitored via spectrophotometry using AuNPs as catalyst, and further a non-enzymatic sensor was fabricated. The results demonstrated that AuNPs presented excellent catalytic activity and provided a sensitive response to H$_2$O$_2$ detection.

**Keywords:** gold nanoparticles; alginate; catalytic activity

## 1. Introduction

Gold nanoparticles (AuNPs) have recently received intensive interest because of their unique physicochemical properties and their various potential chemical applications [1–3]. However, despite these advantages, AuNPs synthesis usually involves chemical reduction reaction in the presence of various reducing agents and capping agents, in which toxic chemicals are used [4–6]. Therefore, development of an efficient, green, and eco-friendly method to prepare AuNPs is a worthy endeavor. Studies have reported that many natural compounds, such as those derived from fungi, algae, bacteria, and plants, were used in green synthesis of AuNPs [7–10]. These natural compounds-mediated procedures for synthesis of AuNPs represent advantages over conventional chemical and physical methods, as they are simply, low-cost, energy-efficient, and nontoxic green routes [11–14]. In this regard, we focused our attention on natural polysaccharide extracted from seaweed, which is a proven source of bioactive compounds [15]. Furthermore, natural polysaccharides can be used for AuNPs synthesis in a different way [16]. Alginate, one kind of polysaccharide, isolated from marine algae, is a biocompatible, non-toxic, and biodegradable compound. Alginate is a copolymer of β-D-mannuronic acid (M) and α-L-guluronic acid (G) and has a number of free carboxyl and hydroxyl groups distributed along its backbone [17,18]. In the preparation of the AuNPs, the hydroxyl groups of alginate can reduce the Au (III) ions to Au (0). Meanwhile, the interaction between Au

and functional groups such as hydroxyl and carboxyl groups prevented AuNPs from aggregation and provided smaller AuNPs. Recently, several researchers reported the synthesis of AuNPs with alginate [19–21]. Nevertheless, few studies report the applications of AuNPs-algiante in catalytic reduction of 4-nitrophenol (4-NP) and sensor preparation for detecting $H_2O_2$.

The present work reports on AuNPs synthesis via a facile solvothermal method with alginate as both reducing and stabilizing agent. Furthermore, this work discusses the application of these newly synthesized AuNPs in catalytic reduction of 4-nitrophenol (4-NP). 4-NP is one of the most common hazardous organic pollutants and contaminates the environment. While, the reduced product, 4-nitroaniline (4-AP) is a very important intermediate for the production various drugs, dyeing agent, photographic developers, and corrosion inhibitors [22,23]. Nonetheless, the reduction of 4-NP by traditional methods are mostly ineffective due to the high stability and low solubility of 4-NP in water. Therefore, direct catalytic reduction of 4-NP into 4-AP using a facile and efficient method is indispensable in the present day context.

Additionally, most previous studies indicate that hydrogen peroxide ($H_2O_2$) is an important intermediate species in food, pharmaceutical, industrial, and environmental analysis, but, bioaccumulation of $H_2O_2$ produces oxidative stress and results in severe damage to cells [24,25]. Nowadays, considerable attention has been focused on rapid, low-cost, accurate determination of $H_2O_2$ in trace levels in biological and various water samples [26–28]. Many analytical methods have been developed to detect $H_2O_2$, such as chemiluminescence, spectrophotometry, titrimetry and electrochemical method. Among them, non-enzymatic electrochemical sensors are attracted much attention due to its advantages of low-cost, simplicity, high sensitivity and high selectivity [29–31]. The standard reduction potential for the reaction of $H_2O_2$ is 1.77 V, and AuNPs, as a typical noble metal NPs, has been reported to exhibit good catalytic activity toward the reduction of $H_2O_2$ [32]. Unfortunately, a great number of AuNPs tend to easily aggregate and change shape due to the poor balance between the nucleation and growth processes and the high surface energy, which results in a remarkable decrease in their catalytic and electrochemical activity and selectivity undesirably. To overcome these obstacles, in this study, AuNPs were stabled and dispersed by alginate. non-enzymatic $H_2O_2$ sensor was fabricated with the as-prepared alginate-AuNPs and electrochemical property of the sensor was investigated.

## 2. Experimental Section

Sodium alginate (SA) was supplied by Jiejing Seaweed Co. Ltd., Rizhao, Shandong Province, China. Analytical grade chloroauric acid ($HAuCl_4$), 4-nitrophenol (4-NP) and sodium borohydride ($NaBH_4$) were supplied by Beijing Chemical Factory (Beijing, China) and used as supplied without further purification. All solutions were prepared with deionized water.

In a typical preparation, sodium alginate was dissolved in distilled water. After alginate was completely dissolved, certain amount of chloroauric acid ($HAuCl_4$, 24 mM) precursor was added drop-wise into 5 mL of sodium alginate solution. The reaction mixture was subsequently heated to facilitate the reduction of gold ions.

UV-vis spectra of AuNPs in alginate solution were obtained on a Shimadzu UV3150. Transmission electron microscopy (TEM) images were obtained by a JEM-1200EX microscope at an accelerating voltage of 100.0 kV. X-ray diffraction (XRD) measurements were performed on a powder X-ray diffractometer (D/MAX-RB) using CuKα radiation (λ = 0.15418 nm) over a 2θ range of 5°–80°. Particle size distribution and zeta potential was measured by Differential Light Scattering (DLS) Malvern Zetasizer Nano ZS (Malvern Instruments Ltd., Worcestershire, UK).

We chose the reduction of 4-NP by $NaBH_4$ as a model reaction to evaluate the catalytic activity of the prepared AuNPs. First, 4.5 mL of freshly prepared 0.05 M $NaBH_4$ aqueous solution was mixed with 0.5 mL of 1 mM 4-NP aqueous solution. Subsequently, 20 μL of alginate-AuNPs solution was added into the mixture. The conversion of 4-NP into 4-AP at room temperature was monitored by a UV-vis spectrophotometer (Shimadzu UV3150, Kyoto, Japan).

Electrochemical measurements were performed at room temperature with a conventional three-electrode system controlled by a CHI 760E electrochemical workstation (Shanghai CH Instrument Co. Ltd., Shanghai, China). A platinum coil and a saturated calomel electrode (SCE) were used as the counter and reference electrodes, respectively. The glassy carbon electrode (GCE) was used as working electrode, which was surface modified with the prepared materials. The GCE (4.0 mm in diameter) was firstly polished with 0.3 and 0.05 mm alumina slurries on a polishing cloth and then rinsed with deionized water, followed by ultrasonic treatment in deionized water and ethanol successively. Au suspension (5 μL), which was prepared using 1.0 mM HAuCl$_4$, was dropcasted on the cleaned GCE and dried in air at room temperature. The modified electrodes were identified as AuNPs/GCE.

Scheme 1 shows a schematic diagram of the formation of AuNPs with alginate, as well as the catalytic hydrogenation of 4-NP to 4-AP and the fabrication of the non-enzymatic H$_2$O$_2$ sensor.
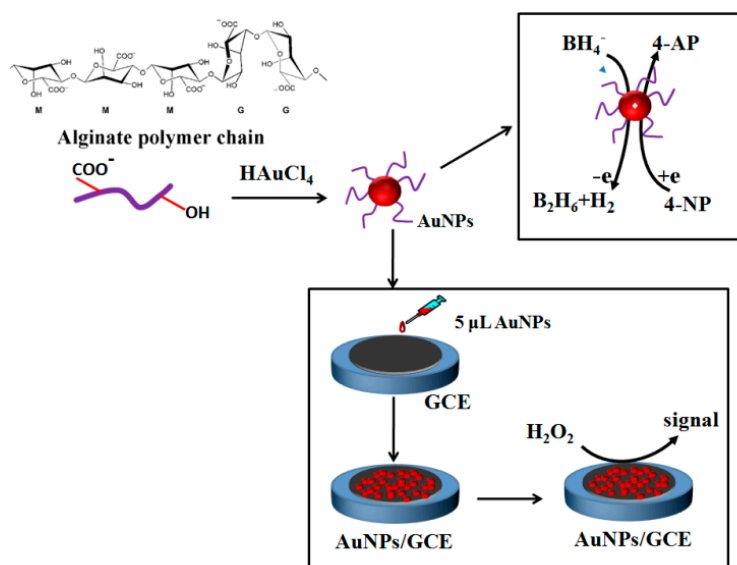


**Scheme 1.** Schematic illustration of the formation of AuNPs with alginate and its application for the catalytic hydrogenation of 4-NP to 4-AP and the non-enzymatic H$_2$O$_2$ sensor.

## 3. Results and Discussion

### 3.1. Effect of Reaction Parameters on the Synthesis of Gold Nanoparticles

During heating, the color of sodium alginate solutions containing HAuCl$_4$ changed slowly from yellow to pink resulting from the reduction of Au$^{3+}$ into Au$^0$ (Figure S1) [33]. UV-vis spectroscopic analysis was used to measure AuNPs formation. Figure 1A shows the UV-vis spectra of the AuNPs obtained using different concentrations (0.1–2%) of sodium alginate as reducing and stabilizing agent. The spectra showed a unique localized surface plasmon resonance (LSPR) absorption band at approximately 520–550 nm, which is associated with AuNPs formation. This result indicated that Au$^{3+}$ could be reduced into Au$^0$ by alginate due to the presence of hydroxyl (OH) groups in the polymer chain [34]. The absorption intensity increased rapidly with increased sodium alginate concentration, and this phenomenon could be attributed to the high amount of OH groups in alginate; these OH groups facilitate the reduction of Au$^{3+}$, increasing AuNPs yield. The peak shifted toward shorter wavelength from 550 nm to 530 nm at increased alginate concentrations, indicating that the nanoparticles were well dispersed in the reactive system resulting from the stabilizing effect of alginate. Sardar et al. reported that at higher polymer concentration the initial rate of formation of AuNPs was slower and the reduction took a longer time to complete. Alginate probably formed a micelle around Au$^0$ nuclei, as a result, alginate could control the growth of particles [35,36].

Preparation of AuNPs using 1.0% sodium alginate was evaluated under varying $HAuCl_4$ concentrations, and the UV-vis spectra of the AuNPs obtained are shown in Figure 1B. A significant LSPR absorbance peak was centered at approximately 530 nm. With increasing Au atomic ratio, the LSPR band of AuNPs enhanced first and then decreased. This phenomenon may be attributed to change in size of the AuNPs as revealed in their TEM image. With increasing Au content, the AuNPs probably reunited and enlarged, causing the visible light absorbance to decrease, the broadening of the peak may results from increasing the polydispersity of AuNPs [36,37].

The gold nanoparticles formation was examined at different time intervals. With the passage of time from 20 to 40 min, the intensity of absorbance peaks increased and broadness of absorbance peaks decreased as shown in Figure 1C, reflecting the formation of more AuNPs. While, further prolonging the reaction duration up to 60 min, the intensity of plasmon absorption band displayed a slight decrease, also, the maximum of the absorbance peak was nearly the same, implying the as-prepared aqueous dispersions of AuNPs were very stable against aggregation. Figure 1D showed the UV–vis absorption spectroscopy of AuNPs prepared at different temperatures using 1.0% sodium alginate and 1.2 mM $HAuCl_4$. It was clear from the data that the temperature played the important role to the reduction reaction and particle size, when the reaction temperature was 50 °C–70 °C, the intensity of the plasmon band was weak and very broaden around 570 nm, which indicated that the reduction efficiency was not very good and no complete transformation of $Au^{3+}$ into gold nanopartricles was achieved at this temperature. Raising the reaction temperature up to 80 °C, the absorption band at 526 nm becomes stronger and narrower which means higher conversion of $Au^{3+}$ to $Au^0$ with smaller nanoparticles size. This might result from the reduction of Au ions by alginate molecules at higher temperature [35]. As Wang et al. reported, fast nucleation yielded smaller particles and higher particle concentration at higher temperature [38]. On the other hand, there was significant enhancement in the absorption band by rising the temperature up to 100 °C with concomitant wavelength shifted towards larger wavelength band (535 nm), indicating that larger nanosized gold were formed [39]. The possible reason is the degradation of alginate at higher temperature, resulting in the higher reducing capacity and lower stabilizing power to AuNPs.
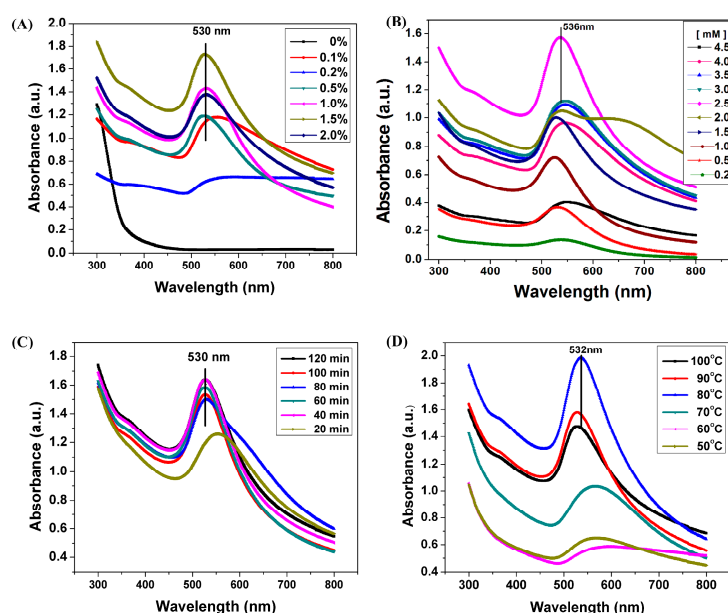


**Figure 1.** Effect of reaction parameters on the synthesis of gold nanoparticles. (**A**) UV-vis spectra of AuNPs prepared using different concentrations of sodium alginate in the presence of $HAuCl_4$ (2.5 mM) at 90 °C for 60 min; (**B**) UV-vis spectra of AuNPs prepared using different concentrations of $HAuCl_4$, sodium alginate (1.0%) at 90 °C for 60 min; (**C**) UV-vis spectra of AuNPs prepared at different reaction time with sodium alginate 1.0%, $HAuCl_4$ 1.2 mM at 90 °C; (**D**) UV-vis spectra of AuNPs prepared with different reaction temperature with sodium alginate 1.0%, $HAuCl_4$ 1.2 mM, 60 min.

### 3.2. TEM, XRD and DLS Analysis

The TEM images (Figure 2A–C) provided information on the size, morphology and dispersion of the obtained AuNPs under different concentrations of $HAuCl_4$. The AuNPs mainly assumed a nearly spherical shape at low $HAuCl_4$ concentration. Additionally, the size of AuNPs varied under different concentrations of $Au^{3+}$ ions. The histograms (the inset of Figure 2A–C) clearly illustrated that the prepared particle size was around 10 nm at low concentrations of $HAuCl_4$. While, the formed AuNPs tended to aggregate when the concentration of $HAuCl_4$ was increased up to 3.5 mM, large particles were found and the NPs varied from 10 to 60 nm in size. The crystalline nature of the prepared AuNPs was confirmed by wide-angle XRD analysis, and the result was shown in Figure 2D. Several distinct diffraction peaks at approximately 38.2°, 44.4°, 64.6°, and 77.6° were assigned to the reflections from the (1 1 1), (2 0 0), (2 2 0), and (3 1 1) planes of Au crystal, respectively; these peaks corroborate the crystalline structure of AuNPs and further on the basis that they can be indexed as face-centered-cubic (FCC) structure of Au [40]. Among the corresponding planes, (1 1 1) plane exhibited a higher intensity than the other planes, suggesting that the (1 1 1) plane is the predominant orientation. The intensity of the diffraction peaks varies with increasing concentration of $HAuCl_4$.
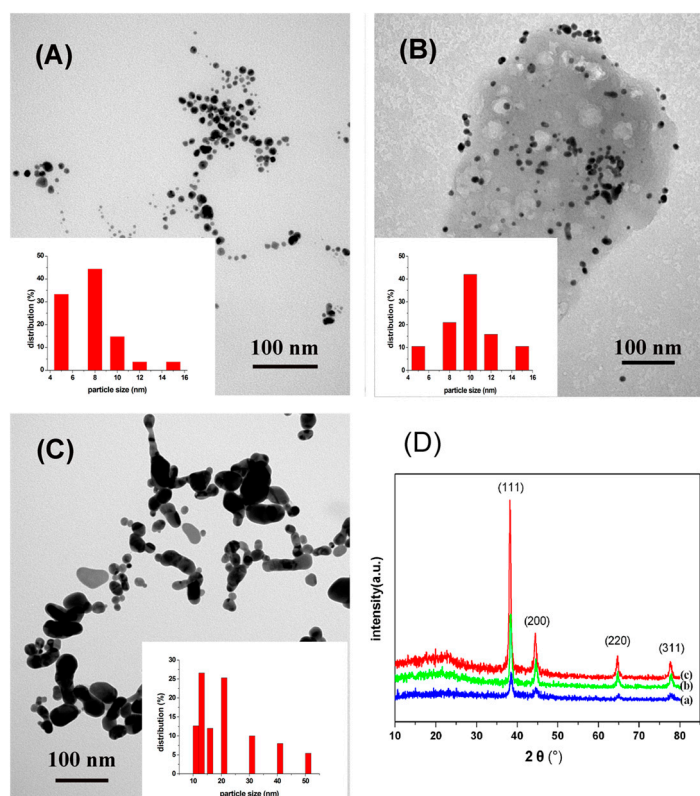


**Figure 2.** (**A**–**C**) TEM images of AuNPs prepared using 0.25, 1.0, 3.5 mM of $HAuCl_4$, respectively; (**D**) XRD patterns of AuNPs prepared using different $HAuCl_4$ concentrations of 0.25 (**a**); 1.0 (**b**); 3.5 (**c**) mM, respectively. The inset is the corresponding particle size analysis histogram of the gold nanoparticles.

Dynamic light scattering (DLS) analysis showed the size distribution by number of particles obtained under different concentrations of $HAuCl_4$ (Figure 3). The average particle size determined by DLS method was slightly increased from 7 nm to 9 nm at lower $HAuCl_4$ concentration (Figure 3A,B). While, the particle size increased to be 50 nm with the increase of $HAuCl_4$ concentration up to 3.5 mM. The result is in agreement with the result obtained from TEM. Additionally, a stable dispersion of particles was evident from the zeta potential of −52.3 mV (Figure 4); a zeta potential higher than 30 mV or lesser than −30 mV indicates a stable system [3,41]. Additionally, the stabilization of the

AuNPs is not only due to electrostatic phenomenon, but also the polymeric structure of alginate [38,42]. Alginate can act as surface active molecules to stabilize the nanoparticles due to the extensive number of hydroxyl and carboxylic groups on alginate chain. However, further studies are required to elucidate the mechanism of biological AuNPs synthesis.
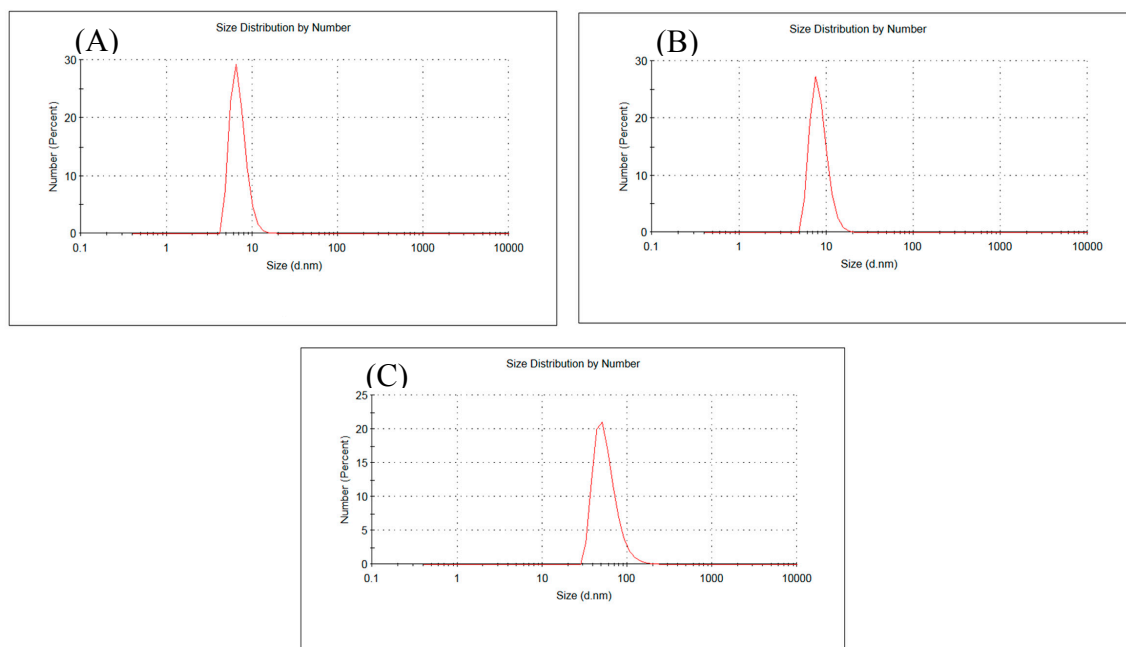


**Figure 3.** (**A–C**) DLS profile: Size distribution by number of AuNPs prepared using 0.25, 1.0, 3.5 mM HAuCl$_4$, respectively.
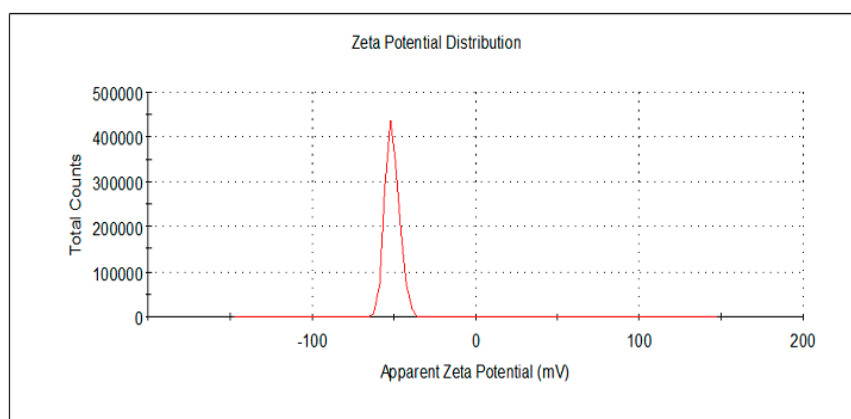


**Figure 4.** Zeta potential analysis of AuNPs prepared using 0.25 mM HAuCl$_4$.

*3.3. Catalytic Activity Study of Gold Nanoparticles*

This work investigated the catalytic activity of AuNPs in reduction of 4-NP into 4-AP in the presence of NaBH$_4$. Reduction of 4-NP by NaBH$_4$ is thermodynamically feasible involving a standard reduction potential of $-0.76$ for 4-NP/4-AP and $-1.33$ V for H$_3$BO$_3$/BH$_4^-$ versus that of a normal hydrogen electrode; however, this reaction is kinetically restricted in the absence of a catalyst [43]. The color of 4-NP solution changed from light yellow to bright yellow immediately upon addition of NaBH$_4$ solution, and the absorption peak of 4-NP shifted from 317 nm to 400 nm, which was due to the formation of 4-nitrophenolate ions under highly basic conditions (Figure S2). The absorbance of 4-NP at 400 nm decreased only slightly in the absence of a catalyst, suggesting that 4-NP was not effectively

reduced by $NaBH_4$ or that the reduction rate was very slow (Figure S3). By contrast, after adding AuNPs into the reaction medium, the absorption peak of 4-NP at 400 nm decreased abruptly, along with the appearance of a new absorption peak of 4-AP at 300 nm (Figure 5A–C), indicating the successful reduction of 4-NP into 4-AP. Moreover, the AuNP catalyst exhibited an efficient catalytic activity within 12 min to nearly the completion of the reaction. AuNPs act as electron relay center and initiate shifting of electron from the donor $BH_4^-$ to the acceptor 4-NP, causing reduction of 4-NP. The reactant molecules ($BH_4^-$ ion and 4-NP) were simultaneously adsorbed onto the surface of NPs, as a result, electrons transferred from $BH_4^-$ ion into 4-NP through the NPs [44].

Reduction of 4-NP fits well a pseudo-first order kinetics equation when the amount of $NaBH_4$ in the reaction medium is excessive compared with that of 4-NP. Thus, $\ln(A_t/A_0) = -kt$, where $A_t/A_0$ is the ratio of the absorbance at 400 nm of 4-NP at time t to that at time 0, k is the rate constant of the reaction, and t is the reaction time (min). The value of k could be determined from the slopes between $\ln(A_t/A_0)$ versus t. The plots of $\ln(A_t/A_0)$ versus time for the reduction of 4-NP by $NaBH_4$ with varied forms of AuNPs as catalysts are shown in Figure 5D. Obviously, a good linear relationship between $\ln(A_t/A_0)$ versus time was observed, confirming pseudo-first-order kinetics. The corresponding rate constants k are 0.331, 0.314, and 0.492 min when AuNPs prepared with 0.25 (a), 1.0 (b), 3.5 (c) mM $HAuCl_4$ were used, respectively. A study has shown that k is related to the total surface area of AuNPs, which depends on the size and content of AuNPs [45]. A considerably increased amount of AuNPs that formed at high $HAuCl_4$ concentration will increase the catalytic activity, whereas, the increased particle size will reduce the catalytic activity.
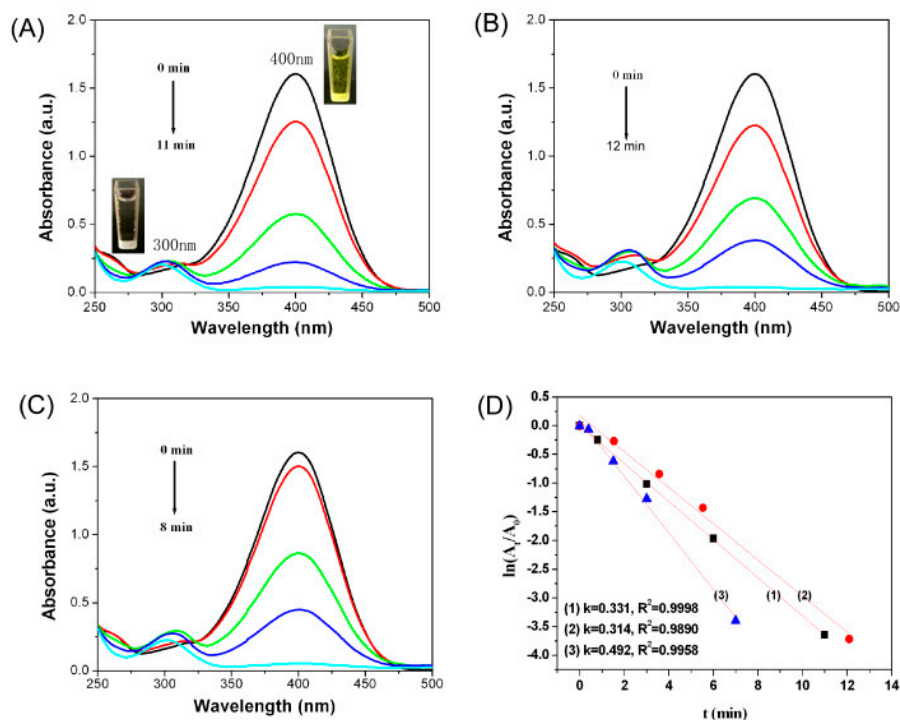


**Figure 5.** (**A–C**) Time-dependent absorption spectra of the reaction solution of 4-NP into 4-AP over AuNPs prepared using 0.25, 1.0, and 3.5 mM $HAuCl_4$, respectively; (**D**) (1), (2), and (3) show the plot of $\ln(A_t/A_0)$ against the reaction time over AuNPs prepared using 0.25, 1.0, and 3.5 mM $HAuCl_4$, respectively.

## 3.4. Catalytic Activity Study of Gold Nanoparticles

To testify the sensing application of as-prepared AuNPs, an enzymeless $H_2O_2$ sensor has been constructed by direct deposition of the AuNPs aqueous dispersion on a bare GCE surface. The electrocatalytic activity of AuNPs modified electrodes toward $H_2O_2$ oxidation was studied

using typical cyclic voltammetry (CV). According to the literature [30,46], the mechanism of $H_2O_2$ electroreduction can be summarized as the following sequence:

$$H_2O_2 + e^- \leftrightarrow OH_{(ads)} + OH^-$$

$$OH_{(ads)} + e^- \leftrightarrow OH^-$$

$$2OH^- \cdot + H^+ \leftrightarrow 2H_2O$$
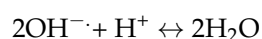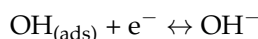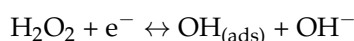
Importantly, when AuNPs was introduced in the reaction, it became more irreversible. The possible reaction may be obeyed the following equations [26,30]:

$$H_2O_2 \rightarrow 1/2\, O_2 + H_2O$$
$$O_2 + 2e^- + 2H^+ \rightarrow H_2O_2 \tag{1}$$

The electrocatalytic detection of $H_2O_2$ should be attributed to the reduction of $H_2O_2$ on the AuNPs surface. The oxygen generated in the reaction was turned into the detection signal at the electrode.

The catalytic responses of the AuNPs modified GCE by changing the concentration of $H_2O_2$ in $N_2$-saturated 0.1 M PBS solution (pH 7.2) at scan rate of 50 mV s$^{-1}$ were recorded in Figure 6A. It can be seen that only a featureless CV profile was obtained when no $H_2O_2$ was introduced in the system. After adding $H_2O_2$, the reduction current of $H_2O_2$ increased gradually with the increase of concentration in the range of 0–6 mM, which suggests that the material is electrochemically sensitive to the concentration of $H_2O_2$ [47]. The inset of Figure 6A displays a good linear relationship between the peak current and $H_2O_2$ concentration from 0 to 6 mM ($R^2$ = 0.9888). To explore the reaction kinetics of $H_2O_2$ reduction on the AuNPs, the corresponding CV curves of the AuNPs/GCE scanned at different scan rates in $N_2$-saturated 0.1 M PBS solution with 3 mM $H_2O_2$ are shown in Figure 6B. It can be seen the reduction current increases gradually with the scan rate increased from 50 to 400 mV s$^{-1}$. As shown in the inset of Figure 6B, the peak current shows a linear increase to the square root of scan rate, indicating that the reduction reaction of $H_2O_2$ is a diffusion-controlled process [48].
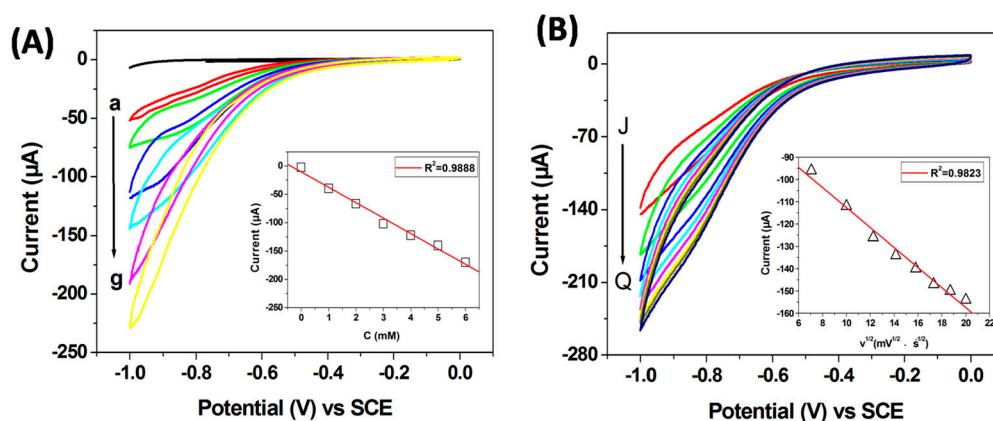


**Figure 6.** (**A**) CV curves of AuNPs/GCE obtained in $N_2$-saturated 0.1 M PBS (pH 7.2) with different $H_2O_2$ concentration (from a to g: 0, 1, 2, 3, 4, 5 and 6 mM) at a 50 mV S$^{-1}$ scan rate, the inset is the linear fitting program of the reduction peak current (0.9 V) versus the $H_2O_2$ concentration; (**B**) CV curves of AuNPs/GCE obtained in $N_2$-saturated 0.1 M PBS (pH 7.2) containing 3 mM $H_2O_2$ concentration with different scan rate (from J to Q: 50, 100, 150, 200, 250, 300, 350 and 400 mV S$^{-1}$), the inset is the linear fitting program of the reduction peak current (0.9 V) versus the square root of scan rate.

## 4. Conclusions

AuNPs were synthesized using sodium alginate via a facile and green method, wherein alginate served as reducing and stabilizing agent. Sodium alginate and HAuCl$_4$ concentrations, as well

as reaction time and temperature exerted obvious effects on AuNPs formation. The synthesized NPs showed pronounced catalytic activity in reduction of 4-NP into 4-APin the presence of $NaBH_4$. The non-enzymatic $H_2O_2$ sensor based on Au/GCE exhibited excellent sensing performances for non-enzymatic $H_2O_2$ detection.

**Author Contributions:** Xihui Zhao designed the experiments and wrote most of the paper; Zichao Li and Yujia Deng contributed to the analysis experimental data and the writing of the paper; Zhihui Zhao performed DLS experiments and contributed to the analysis of the data; Xiaowen Li contributed to the discussions of experimental results; Yanzhi Xia conceived the structure of the manuscript; All of the authors were involved in the conception and experiment design as well as the discussion of the results and the writing of the manuscript.

**Conflicts of Interest:** The authors declare no conflict of interest.

## References

1. El-Naggar, M.E.; Shaheen, T.I.; Fouda, M.M.G.; Hebeish, A.A. Eco-friendly microwave-assisted green and rapid synthesis of well-stabilized gold and core-shell silver-gold nanoparticles. *Carbohydr. Polym.* **2016**, *136*, 1128–1136. [CrossRef] [PubMed]

2. Talib, A.; Khan, M.S.; Gedda, G.; Wu, H.F. Stabilization of gold nanoparticles using natural plant gel: A greener step towards biological applications. *J. Mol. Liq.* **2016**, *220*, 463–467. [CrossRef]

3. Anand, K.; Gengan, R.M.; Phulukdaree, A.; Chuturgoon, A. Agroforestry waste moringa oleifera petals mediated green synthesis of gold nanoparticles and their anti-cancer and catalytic activity. *J. Ind. Eng. Chem.* **2015**, *21*, 1105–1111. [CrossRef]

4. Alex, S.; Tian, K.; Teng, S.; Siegel, G.; Tiwari, A. Simple and rapid green synthesis of micrometer scale single crystalline gold nanoplates using chitosan as the reducing agent. *J. Cryst. Growth* **2014**, *406*, 12–17. [CrossRef]

5. Hwang, S.J.; Jun, S.H.; Park, Y.; Cha, S.H.; Yoon, M.; Cho, S.; Lee, H.J. Green synthesis of gold nanoparticles using chlorogenic acid and their enhanced performance for inflammation. *Nanomed. Nanotechnol. Biol. Med.* **2015**, *11*, 1677–1688. [CrossRef] [PubMed]

6. Binupriya, A.R.; Sathishkumar, M.; Vijayaraghavan, K.; Yun, S.I. Bioreduction of trivalent aurum to nano-crystalline gold particles by active and inactive cells and cell-free extract of aspergillus oryzae var. viridis. *J. Hazard. Mater.* **2010**, *177*, 539–545. [CrossRef] [PubMed]

7. Paul, B.; Bhuyan, B.; Purkayastha, D.D.; Dey, M.; Dhar, S.S. Green synthesis of gold nanoparticles using *Pogestemon benghalensis*(b) O. Ktz. Leaf extract and studies of their photocatalytic activity in degradation of methylene blue. *Mater. Lett.* **2015**, *148*, 37–40. [CrossRef]

8. Sharma, B.; Purkayastha, D.D.; Hazra, S.; Gogoi, L.; Bhattacharjee, C.R.; Ghosh, N.N.; Rout, J. Biosynthesis of gold nanoparticles using a freshwater green alga, prasiola crispa. *Mater. Lett.* **2014**, *116*, 94–97. [CrossRef]

9. Iravani, S. Green synthesis of metal nanoparticles using plants. *Green Chem.* **2011**, *13*, 2638–2650. [CrossRef]

10. Singaravelu, G.; Arockiamary, J.S.; Kumar, V.G.; Govindaraju, K. A novel extracellular synthesis of monodisperse gold nanoparticles using marine alga, sargassum wightii greville. *Colloids Surf. B Biointerfaces* **2007**, *57*, 97–101. [CrossRef] [PubMed]

11. Gonzalez-Ballesteros, N.; Prado-Lopez, S.; Rodriguez-Gonzalez, J.B.; Lastra, M.; Rodriguez-Arguelles, M.C. Green synthesis of gold nanoparticles using brown algae cystoseira baccata: Its activity in colon cancer cells. *Colloids Surf. B Biointerfaces* **2017**, *153*, 190–198. [CrossRef] [PubMed]

12. Shi, G.; Li, Y.; Xi, G.; Xu, Q.; He, Z.; Liu, Y.; Zhang, J.; Cai, J. Rapid green synthesis of gold nanocatalyst for high-efficiency degradation of quinclorac. *J. Hazard. Mater.* **2017**, *335*, 170–177. [CrossRef] [PubMed]

13. Ghodake, G.S.; Deshpande, N.G.; Lee, Y.P.; Jin, E.S. Pear fruit extract-assisted room-temperature biosynthesis of gold nanoplates. *Colloids Surf. B Biointerfaces* **2010**, *75*, 584–589. [CrossRef] [PubMed]

14. Bagci, P.O.; Wang, Y.-C.; Gunasekaran, S. A simple and green route for room-temperature synthesis of gold nanoparticles and selective colorimetric detection of cysteine. *J. Food Sci.* **2015**, *80*, N2071–N2078. [CrossRef] [PubMed]

15.　Zafar, R.; Zia, K.M.; Tabasum, S.; Jabeen, F.; Noreen, A.; Zuber, M. Polysaccharide based bionanocomposites, properties and applications: A review. *Int. J. Biol. Macromol.* **2016**, *92*, 1012–1024. [CrossRef] [PubMed]

16.　Wang, C.Y.; Huan, K.S.; Yang, C.H.; Chang, W.R.; Grumezescu, A.M. A facile synthesis of gold nanoparticles-alginate composite spheres. *Int. J. Latest Res. Sci. Technol.* **2014**, *3*, 139–142.

17.　Qin, Y. Alginate fibres: An overview of the production processes and applications in wound management. *Polym. Int.* **2008**, *57*, 171–180. [CrossRef]

18.　Sikorski, P.; Mo, F.; Skjak-Braek, G.; Stokke, B.T. Evidence for egg-box-compatible interactions in calcium-alginate gels from fiber X-ray diffraction. *Biomacromolecules* **2007**, *8*, 2098–2103. [CrossRef] [PubMed]

19.　Li, Y.; Li, G.; Li, W.; Yang, F.; Liu, H. Greenly synthesized gold-alginate nanocomposites catalyst for reducing decoloration of azo-dyes. *Nano* **2015**, *10*. [CrossRef]

20.　Nguyen Tue, A.; Van Dang, P.; Nguyen Ngoc, D.; Bui Duy, D.; Nguyen Quoc, H. Synthesis of alginate stabilized gold nanoparticles by gamma-irradiation with controllable size using different $Au^{3+}$ concentration and seed particles enlargement. *Radiat. Phys. Chem.* **2010**, *79*, 405–408.

21.　Saha, S.; Pal, A.; Kundu, S.; Basu, S.; Pal, T. Photochemical green synthesis of calcium-alginate-stabilized Ag and Au nanoparticles and their catalytic application to 4-nitrophenol reduction. *Langmuir* **2010**, *26*, 2885–2893. [CrossRef] [PubMed]

22.　Hu, H.; Xin, J.H.; Hu, H. Pam/graphene/Ag ternary hydrogel: Synthesis, characterization and catalytic application. *J. Mater. Chem. A* **2014**, *2*, 11319–11333. [CrossRef]

23.　Li, Y.; Cao, Y.; Xie, J.; Jia, D.; Qin, H.; Liang, Z. Facile solid-state synthesis of ag/graphene oxide nanocomposites as highly active and stable catalyst for the reduction of 4-nitrophenol. *Catal. Commun.* **2015**, *58*, 21–25. [CrossRef]

24.　Li, D.; Meng, L.Y.; Dang, S.C.; Jiang, D.L.; Shi, W.D. Hydrogen peroxide sensing using $Cu_2O$ nanocubes decorated by Ag-Au alloy nanoparticles. *J. Alloys Compd.* **2017**, *690*, 1–7. [CrossRef]

25.　Dong, S.Y.; Yang, Q.X.; Peng, L.; Fang, Y.; Huang, T.L. Dendritic Ag@Cu bimetallic interface for enhanced electrochemical responses on glucose and hydrogen peroxide. *Sens. Actuators B Chem.* **2016**, *232*, 375–382. [CrossRef]

26.　Zhang, Y.; Wang, Z.Y.; Liu, S.; Zhang, T. In situ growth of ag-reduced graphene oxide-carbon nanotube on indium tin oxide and its application for electrochemical sensing. *Mater. Res. Bull.* **2016**, *84*, 355–362. [CrossRef]

27.　Zhang, D.J.; Zhang, J.C.; Zhang, R.C.; Shi, H.Z.; Guo, Y.Y.; Guo, X.L.; Li, S.J.; Yuan, B.L. 3d porous metal-organic framework as an efficient electrocatalyst for nonenzymatic sensing application. *Talanta* **2015**, *144*, 1176–1181. [CrossRef] [PubMed]

28.　Wang, M.Q.; Zhang, Y.; Bao, S.J.; Yu, Y.N.; Ye, C. Ni(ii)-based metal-organic framework anchored on carbon nanotubes for highly sensitive non-enzymatic hydrogen peroxide sensing. *Electrochim. Acta* **2016**, *190*, 365–370. [CrossRef]

29.　Gutierrez, A.; Lozano, M.L.; Galicia, L.; Ferreyra, N.F.; Rivas, G.A. Electrochemical sensing of uric acid using glassy carbon modified with multiwall carbon nanotubes dispersed in polyethylenimine. *Electroanalysis* **2014**, *26*, 2191–2196. [CrossRef]

30.　Li, Z.; Zheng, X.H.; Zheng, J.B. A non-enzymatic sensor based on Au@Ag nanoparticles with good stability for sensitive detection of $H_2O_2$. *New J. Chem.* **2016**, *40*, 2115–2120. [CrossRef]

31.　Zhong, Y.M.; Li, Y.C.; Li, S.X.; Feng, S.Q.; Zhang, Y.Y. Nonenzymatic hydrogen peroxide biosensor based on four different morphologies of cuprous oxide nanocrystals. *RSC Adv.* **2014**, *4*, 40638–40642. [CrossRef]

32.　Li, S.-J.; Shi, Y.-F.; Liu, L.; Song, L.-X.; Pang, H.; Du, J.-M. Electrostatic self-assembly for preparation of sulfonated graphene/gold nanoparticle hybrids and their application for hydrogen peroxide sensing. *Electrochim. Acta* **2012**, *85*, 628–635. [CrossRef]

33.　Konowal, E.; Modrzejewska-Sikorska, A.; Milczarek, G. Synthesis and multifunctional properties of lignosulfonate-stabilized gold nanoparticles. *Mater. Lett.* **2015**, *159*, 451–454. [CrossRef]

34.　Yang, J.; Pan, J. Hydrothermal synthesis of silver nanoparticles by sodium alginate and their applications in surface-enhanced raman scattering and catalysis. *Acta Mater.* **2012**, *60*, 4753–4758. [CrossRef]

35.　Sardar, R.; Park, J.-W.; Shumaker-Parry, J.S. Polymer-induced synthesis of stable gold and silver nanoparticles and subsequent ligand exchange in water. *Langmuir* **2007**, *23*, 11883–11889. [CrossRef] [PubMed]

36. Sardar, R.; Shumaker-Parry, J.S. Spectroscopic and microscopic investigation of gold nanoparticle formation: Ligand and temperature effects on rate and particle size. *J. Am. Chem. Soc.* **2011**, *133*, 8179–8190. [CrossRef] [PubMed]

37. Sardar, R.; Heap, T.B.; Shumaker-Parry, J.S. Versatile solid phase synthesis of gold nanoparticle dimers using an asymmetric functionalization approach. *J. Am. Chem. Soc.* **2007**, *129*, 5356–5357. [CrossRef] [PubMed]

38. Wang, Y.-C.; Gunasekaran, S. Spectroscopic and microscopic investigation of gold nanoparticle nucleation and growth mechanisms using gelatin as a stabilizer. *J. Nanopart. Res.* **2012**, *14*, 1–11. [CrossRef]

39. Wang, Y.C.; Lu, L.; Gunasekaran, S. Biopolymer/gold nanoparticles composite plasmonic thermal history indicator to monitor quality and safety of perishable bioproducts. *Biosens. Bioelectron.* **2017**, *92*, 109–116. [CrossRef] [PubMed]

40. Ye, W.C.; Yu, J.; Zhou, Y.X.; Gao, D.Q.; Wang, D.A.; Wang, C.M.; Xue, D.S. Green synthesis of Pt-Au dendrimer-like nanoparticles supported on polydopamine-functionalized graphene and their high performance toward 4-nitrophenol reduction. *Appl. Catal. B Environ.* **2016**, *181*, 371–378. [CrossRef]

41. Rohit, J.V.; Kailasa, S.K. Simple and selective detection of pendimethalin herbicide in water and food samples based on the aggregation of ractopamine-dithiocarbamate functionalized gold nanoparticles. *Sens. Actuators B Chem.* **2017**, *245*, 541–550. [CrossRef]

42. Sardar, R.; Bjorge, N.S.; Shumaker-Parry, J.S. Ph-controlled assemblies of polymeric amine-stabilized gold nanoparticles. *Macromolecules* **2008**, *41*, 4347–4352. [CrossRef]

43. Narayanan, K.B.; Sakthivel, N. Synthesis and characterization of nano-gold composite using cylindrocladium floridanum and its heterogeneous catalysis in the degradation of 4-nitrophenol. *J. Hazard. Mater.* **2011**, *189*, 519–525. [CrossRef] [PubMed]

44. Zhao, X.H.; Li, Q.; Ma, X.M.; Xiong, Z.; Quan, F.Y.; Xia, Y.Z. Alginate fibers embedded with silver nanoparticles as efficient catalysts for reduction of 4-nitrophenol. *RSC Adv.* **2015**, *5*, 49534–49540. [CrossRef]

45. Kuroda, K.; Ishida, T.; Haruta, M. Reduction of 4-nitrophenol to 4-aminophenol over Au nanoparticles deposited on pmma. *J. Mol. Catal. Chem.* **2009**, *298*, 7–11. [CrossRef]

46. Yang, Y.; Fu, R.Z.; Yuan, J.J.; Wu, S.Y.; Zhang, J.L.; Wang, H.Y. Highly sensitive hydrogen peroxide sensor based on a glassy carbon electrode modified with platinum nanoparticles on carbon nanofiber heterostructures. *Microchim. Acta* **2015**, *182*, 2241–2249. [CrossRef]

47. Zhang, M.R.; Chen, X.Q.; Pan, G.B. Electrosynthesis of gold nanoparticles/porous gan electrode for non-enzymatic hydrogen peroxide detection. *Sens. Actuators B Chem.* **2017**, *240*, 142–147. [CrossRef]

48. Li, W.Z.; Kuai, L.; Qin, Q.; Geng, B.Y. Ag-Au bimetallic nanostructures: Co-reduction synthesis and their component-dependent performance for enzyme-free $H_2O_2$ sensing. *J. Mater. Chem. A* **2013**, *1*, 7111–7117. [CrossRef]